Homonuclear dipolar decoupling in solid-state nuclear magnetic resonance under the regime of moderate to high magic-angle spinning frequencies: A status report

Subhradip Paul AND P. K. Madhu[a]

Abstract | We review here the status of homonuclear dipolar decoupling in solid-state nuclear magnetic resonance. With the advent of probes capable of high spinning frequencies, the focus of methodology development emphasises on the applicability of the pulse sequences in the moderate to ultra-fast spinning regime. This review outlines the homonuclear dipolar decoupling sequences that have shown the potential to yield high-resolution ^{1}H spectra at high spinning frequencies.

[a]Corresponding author: P. K. Madhu, Dept. of Chemical Sciences, TIFR, Homi Bhabha Road, Colaba, Mumbai 400 005, India

Department of Chemical Sciences, Tata Institute of Fundamental Research, Homi Bhabha Road, Colaba, Mumbai 400 005, India
madhu@tifr.res.in

Keywords: Solid-State NMR; Homonuclear dipolar decoupling; Lee-Goldburg; PMLG; Symmetry sequences; DUMBO; High MAS frequencies

1. Introduction

In the field of nuclear magnetic resonance (NMR), solid-state NMR has emerged as one of the potential tools for the elucidation of structures of small organic molecules to macromolecules like proteins[1,2]. Structural information, such as resonance assignments and measurement of internuclear distances and angular constraints, have been successfully derived using solid-state NMR[3,4]. Over the years, methodological advances towards improvement in resolution and sensitivity have made it possible to use solid-state NMR in the area of material sciences[5], polymer sciences[6], and biological sciences[7]. The most commonly observed spin-$\frac{1}{2}$ nuclei are ^{13}C, ^{15}N, ^{31}P, and ^{29}Si whilst ^{23}Na and ^{27}Al are the more popular quadrupole nuclei. Resolution and sensitivity enhancement of the NMR signal obtained from these nuclei can be achieved by means of several techniques which have been developed over the years. Some of these are magic-angle spinning (MAS)[8,9], cross-polarisation (CP)[10–12], multiple-quantum coherence excitation schemes[1,14], heteronuclear dipolar decoupling[15–17], double rotation[18], dynamic-angle spinning[19,20], multiple quantum magic-angle spinning[21], satellite transition magic-angle spinning[22], and Car-Purcell-Meiboom-Gill[23]. The techniques which aim at high-resolution spectroscopy involve partial or full averaging of the anisotropic interactions in order to filter out the chemical shifts which can be achieved by a combination of magic-angle spinning, which does averaging in the co-ordinate space, and pulse sequences which do averaging in the spin space.

Protons, being the most abundant nuclei in natural samples, play an important role in NMR spectroscopy and have been widely studied in solution-state NMR. Solid-state NMR spectroscopy of protons is difficult owing to the strong

homonuclear dipolar couplings between them. The high gyromagnetic ratio and 100% abundance of ^{1}H make it impossible for MAS alone to average out the dipolar couplings and to obtain high-resolution spectra. Moreover, unlike chemical-shift anisotropy (CSA) and heteronuclear dipolar couplings (DD_{het}), homonuclear dipolar couplings (DD_{homo}) are homogeneous interactions[24]. So once a proton spin is perturbed, the result is transferred to the entire proton network and hence selective perturbation is very difficult, though not impossible. Hence, MAS alone cannot give high-resolution spectra of protons. In this direction several techniques have been introduced which involve combined rotation and multiple pulse sequences (CRAMPS)[25–27]. Here MAS does spatial averaging and radiofrequency (RF) pulses lead to averaging in spin space.

The first attempt in the field of high resolution ^{1}H spectroscopy was heralded by Lee and Goldburg[28]. After that came many sequences like WHH4 and BLEW12 that mainly relied on averaging in the spin space as the only solution to remove DD_{homo}[26,28,29]. Better theoretical understanding and hardware development have led to the development of further sophisticated sequences[30–34].

In the present day context, the advent of high-spinning probes with spinning frequencies reaching up to 80 kHz, the main interest in methodology has been towards the development of pulse sequences which would perform at high-spinning frequencies using moderate RF power. This would be beneficial for the hardware and prevent heating up of samples. With the aim of increasing the sensitivity of NMR, high magnetic fields have become necessary for big molecules. Hence high spinning frequency is a requirement which would help in averaging out the CSA interactions which increase with the increase in the magnetic field. For the hetero-correlation experiments which involve ^{1}H nuclei to be correlated to any other rare nuclei like ^{13}C or ^{31}P, it is essential to have a high-resolution spectra in the proton dimension.

In this review we will focus mainly on the following issues:

(a). An overview of the homonuclear decoupling sequences with an emphasis on the sequences developed for the high spinning frequencies.

(b). Experimental comparison among these sequences over a span of spinning frequencies.

(c). Certain theoretical insights into these sequences using bimodal Floquet theory[35] or average Hamiltonian theory (AHT)[14,36].

2. Homonuclear dipolar decoupling sequences

Over the years many sequences have been developed for high-resolution ^{1}H spectra in the field of solid-state NMR. We categorise them into:

Group A — Solid-echo based sequences: WHH4[37], MREV8[38], BR24[26], BLEW12[39], DUMBO[32]

Group B — Magic-echo sandwich pulses: TREV8[40], MSHOT3[41,29]

Group C — Lee-Goldburg based sequences: LG[28], FFLG[42], FSLG[43], PMLGn[33], wPMLGn[34]

Group D — Rotor synchronised sequences: $CN_n^{\nu 44}$, $RN_n^{\nu 44}$, SAM[31]

The main focus of this review will be on the DUMBO, wPMLGn, and Group D schemes as it has been demonstrated that these sequences can be used in the regime of high spinning frequencies[30,31,45–49].

2.1. *Solid-echo based sequences*

These sequences have been reviewed in Ref. [50] and here we briefly outline their properties. Details of the setting up of these sequences are well documented in Refs. [36–38]. The basic sequence consists of 90_x-τ-$90_{\bar{y}}$-2τ-90_y-τ-$90_{\bar{x}}$ on-resonance irradiation where 90^o is the flip angle induced by the RF pulse whose phase is denoted by the subscript and τ is the interpulse delay. This basic element constitute the WAHUHA sequence[37] which was further used to build up the sequences MREV8[38], BR24[26], and CORY24[51]. Two other prominent schemes of this group are BLEW12[39] and DUMBO[32]. A schematic of these sequences is given in Fig. 1. Among these sequences DUMBO is a numerically optimised scheme. Initial implementation of BLEW12 and DUMBO involved 2D ^{1}H –^{1}H homo-correlation spectroscopy with the decoupling sequences implemented in the indirect dimension followed by a 90^o excitation pulse and acquisition in the direct dimension. DUMBO can also be implemented in a windowed fashion, thereby reducing the dimensionality of the experiments to 1D from 2D[52]. The DUMBO sequence and its applicability at high spinning frequencies will be discussed later.

Theoretical insights into most of these sequences involved analysis of these sequences using AHT. The time-dependent Hamiltonian of a coupled spin-$\frac{1}{2}$ system can be written as:

$$\mathcal{H}(t) = \mathcal{H}_{ISO} + \mathcal{H}_{CSA}(t) + \mathcal{H}_J + \mathcal{H}_{DD}(t) + \mathcal{H}_{RF}(t) + \mathcal{H}_E(t) \quad (1)$$

Figure 1: Schematics of pulse sequences based on the solid-echo principle of homonuclear dipolar decoupling. The sequences are (a) WHH4, (b) MREV8, (c) BR24, (d) CORY24, (e) BLEW12, and (f) DUMBO. The RF pulses shown here by the rectangular boxes represent 90° pulses with the corresponding phases written on the top of the boxes. The delays τ and 2τ need to be optimised for finite pulse lengths. FID points are collected after each RF cycle for (a–d). The DUMBO sequence is a numerically optimised constant amplitude phase-modulated sequence. The phase modulation is shown in (f).

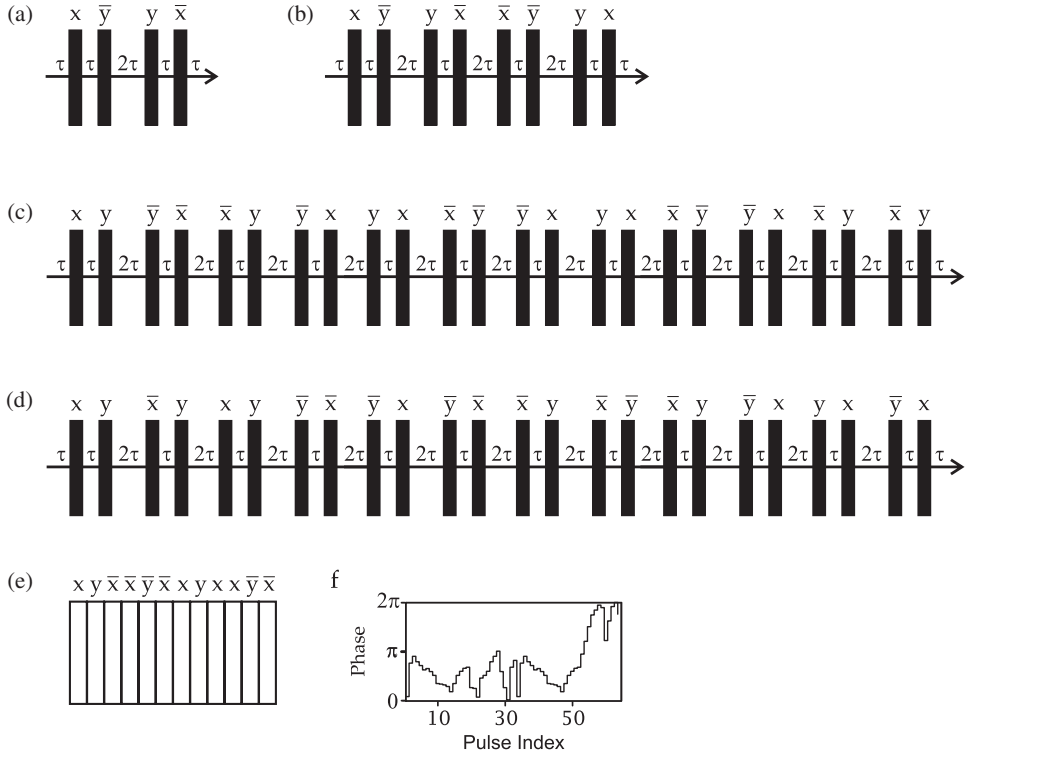

where $\mathcal{H}_{ISO}$, $\mathcal{H}_{CSA}(t)$, $\mathcal{H}_J$, $\mathcal{H}_{DD}(t)$, $\mathcal{H}_{RF}(t)$, and $\mathcal{H}_E(t)$ are the Hamiltonians for isotropic chemical shift, chemical-shift anisotropy (CSA), J-coupling, homonuclear and heteronuclear dipolar interaction, radiofrequency (RF) pulses, and the imperfections present in the RF pulses, respectively. To analyse these sequences using AHT, a similarity transformation needs to be carried out to transform the Hamiltonian into the RF interaction frame given by[36],

$$\widetilde{\mathcal{H}}(t) = U_{RF}^{\dagger}(t)\mathcal{H}(t)U_{RF}(t) \tag{2}$$

with

$$U_{RF}(p\tau_c) = Te^{-i\int_0^{\tau_c} dt'\mathcal{H}_{RF}(t')} = 1 \tag{3}$$

defining the cyclicity of the frame where T is the Dyson time ordering operators, τ_c is the cycle time of the RF sequence, and p is an integer.

From AHT, an effective Hamiltonian $\mathcal{H}_{\text{eff}}$ can be derived which describes the evolution of the spin system. The effective Hamiltonian can be expanded in increasing order of perturbation[39]:

$$\begin{aligned}
\widetilde{\mathcal{H}}_{\text{eff}} &= \widetilde{\mathcal{H}}_{\text{eff}}^{(0)} + \widetilde{\mathcal{H}}_{\text{eff}}^{(1)} + \widetilde{\mathcal{H}}_{\text{eff}}^{(2)} + \cdots \\
\widetilde{\mathcal{H}}_{\text{eff}}^{(0)} &= \widetilde{\mathcal{H}}_{DD}^{(0)} + \widetilde{\mathcal{H}}_{ISO}^{(0)} \\
\widetilde{\mathcal{H}}_{\text{eff}}^{(1)} &= \widetilde{\mathcal{H}}_{DD}^{(1)} + \widetilde{\mathcal{H}}_{CSA}^{(1)} + \widetilde{\mathcal{H}}_{DD\times CSA}^{(1)} \\
\widetilde{\mathcal{H}}_{\text{eff}}^{(2)} &= \widetilde{\mathcal{H}}_{DD}^{(2)} + \widetilde{\mathcal{H}}_{CSA}^{(2)} + \widetilde{\mathcal{H}}_{DD\times CSA}^{(2)} + \cdots
\end{aligned} \tag{4}$$

where $\widetilde{\mathcal{H}}$ represents the Hamiltonian in the RF interaction frame. The upper indices denote the order of perturbation. The lower indices represent the type of interaction and the cross terms between the interactions at higher orders of perturbation. The magnitude of these terms decreases with increasing order of the perturbation.

The terms in Eq. (4) which cause line broadening are $\widetilde{\mathcal{H}}_{DD}^{(0)}$, $\widetilde{\mathcal{H}}_{DD}^{(1)}$, $\widetilde{\mathcal{H}}_{DD\times CSA}^{(1)}$, $\widetilde{\mathcal{H}}_{DD}^{(2)}$, and $\widetilde{\mathcal{H}}_{DD\times CSA}^{(2)}$. The pure CSA terms are ignored here as the CSA

Figure 2: ^{1}H spectra of fumaric acid monoethyl ester at a magnetic field of 4.39 T. The spectra were obtained after a single pulse excitation on (a) static sample and (b) rotating sample. (c) and (d) were obtained implementing BR24 on static sample and under MAS. To keep the τ_r/τ_c ratio less than 5, a MAS frequency of 1.5 kHz to 2.0 kHz was used. (Reproduced with permission from Ref. [41].)

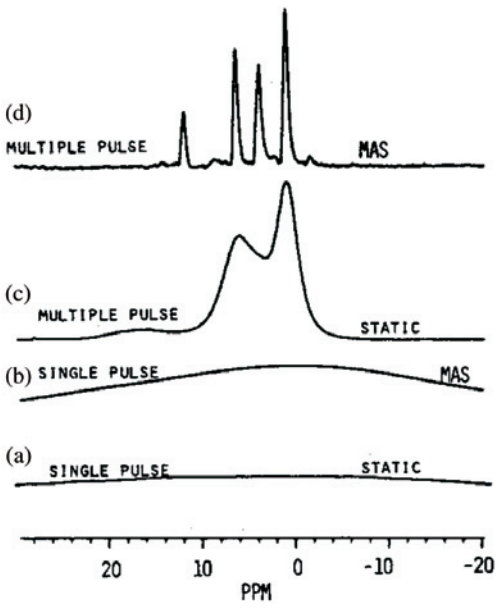

of the protons is small in magnitude. The $\widetilde{\mathcal{H}}^{(0)}_{ISO}$ gives the scaled isotropic chemical shift, the scaling factor being a property of the RF pulse sequence applied. A detailed description of which terms vanish for which sequence is given in Ref. [50]. If we consider 90° pulses of finite length then for all of these sequences except WHH4 and MREV8, $\widetilde{\mathcal{H}}^{(1)}_{DD}$ and $\widetilde{\mathcal{H}}^{(1)}_{DD\times CSA}$ go to zero due to the symmetry of the pulse sequence. The other fact that we have to consider is the magnitude by which the isotropic chemical shift is scaled by these sequences. The scale factor decreases with the increase in the number of RF pulses[50]. So to increase the resolution the line narrowing must be sufficient to compensate for the decrease in the scale factor.

The main problem with these sequences comes from the interference effects due to the presence of the MAS and RF simultaneously. MAS is essential for spatial averaging of the anisotropic interactions. So to avoid interference, it requires that the sequences have a cycle time τ_c which is much shorter than the time taken by the rotor to complete one rotation τ_r. This ensures that the spins do not "feel" the presence of the MAS when the RF pulses are applied. This limit is the "quasi-static" limit[50]. Hence, one of the main drawbacks of these sequences is that they cannot be applied at high MAS frequencies.

Representative spectra of fumaric acid monoethyl ester obtained with BR24 are shown in Fig. 2. They also emphasise the importance of implementing CRAMPS over either MAS or RF alone.

2.2. *Magic-echo sandwich based sequences*

If the time evolution of a spin state under the influence of the homonuclear dipolar interaction can be reversed by the application of suitable RF pulses, then the effect of the interaction can be nullified at the point of the formation of the echo. This has been shown by Rhim et al.[53] and sequences like TERV4[40], TERV8[40], and MSHOT3[29,41] have been developed based on this principle. MSHOT3 was developed from TREV4 by the combination of three TREV4 units with 120° supercycling on them. A schematic of these sequences is shown in Fig. 3.

The magic-echo sandwich based sequences have been reviewed in Ref. [50] and hence without going into details, we will just mention some of the properties of these sequences. The basic symmetric unit for the magic echo or magic sandwich (MS) is given by:

$$\tau\text{-}90^{\circ}_{y}\text{-}360^{\circ}_{x}\text{-}360^{\circ}_{-x}\text{-}90^{\circ}_{y}\text{-}\tau$$

where τ is a delay of length π/ω_1 if ω_1 is the amplitude of the 360° pulse. Assuming 90° δ-pulses, the scale factor of this basic unit is $\frac{1}{3}$.

The most important feature of these sequences is that they are z-rotation sequences. Whilst the pure RF inhomogeneity terms are removed by the reflection symmetry of the subunits of the sequence itself, z-rotation eliminates cross terms arising from the RF inhomogeneity and the dipole-dipole coupling leading to a relatively artifact-free spectra[29]. The first attempt in creating a z-rotation sequence was done by concatenating M subcycles of BLEW12 with the ith subcycle phase shifted by $\phi_i = (i-1)2\pi/M$[29]. The resulting sequence, BHOT4, can eliminate higher-order terms up to fifth order but the main disadvantage of the sequence is that it has a very low scaling factor of 0.186 which makes it practically impossible to apply[29].

In order to avoid low scaling factors, it is mandatory to search for subcycles that can maintain the effective axis of precession close to the z-axis. With the assumption of δ-shaped bracketing pulses $(\frac{\pi}{2})_{\pm y}$, the MS sequence maintains the effective field along the z-axis and eliminates terms of the Hamiltonian corresponding to the irreducible tensors T_{1m} and T_{2m} up to fifth order[29]. Hence MS was chosen to be the building block of the sequences like TREV8 and MSHOT3. The MSHOT3 sequence is built by supercycling three magic-echo units where

Figure 3: Schematic of the (a) TREV8 and (b) MSHOT3 pulse sequences. For ideal δ-shaped pulses, the interpulse delay (τ) has to correspond to the length of a π pulse. For experimental purposes the delay needs to be optimised to compensate for the finite pulse lengths. The phases of the pulses are indicated on top of the pulses whilst the overall flip angle induced is indicated within the rectangular boxes. MSHOT3 pulse sequence was derived by three-step supercycling of the TREV4 units where each consecutive TREV4 units are phase shifted by 120° from one another. The possible sampling points are marked by asterix.

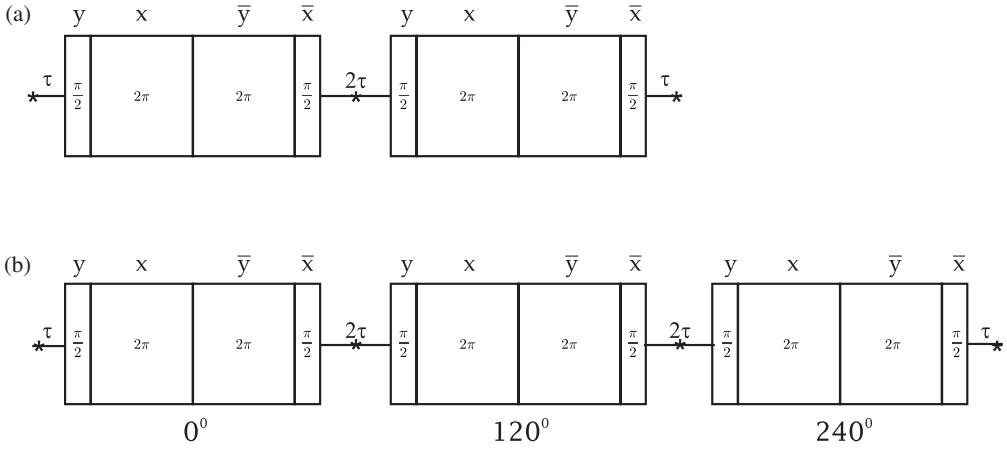

Figure 4: ^{1}H CRAMPS spectra of fumaric acid monoethyl ester obtained with integer number of pulse cycles per rotor period with one sampling point per interval. The homonuclear decoupling sequences used were (a) TREV8 ($\tau_r = 10\tau_c; \omega_r/2\pi = 1595$ Hz), (b) MREV8 ($\tau_r = 12\tau_c; \omega_r/2\pi = 1543$ Hz), (c) BR24 ($\tau_r = 4\tau_c; \omega_r/2\pi = 1543$ Hz), and (d) MSHOT3 ($\tau_r = 5\tau_c; \omega_r/2\pi = 2101$ Hz). The spectra were obtained at a magnetic field of B_0 = 9.4 T and amplitude of the RF power applied was about 119 kHz. (Reproduced with permission from Ref. [26].)

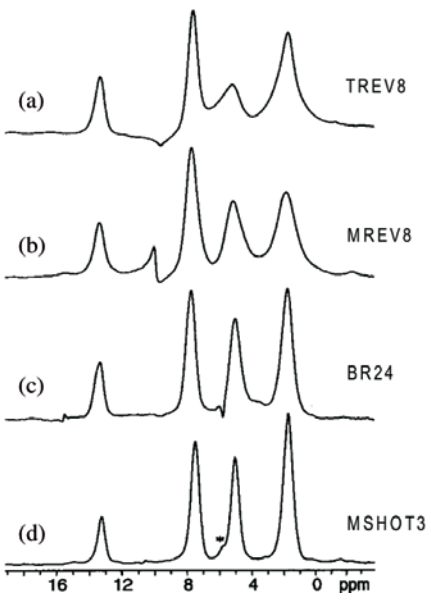

each consequent subunit is phase shifted by 120° as shown in Fig. 3. If we consider finite pulse lengths, then the interpulse delay has to be adjusted to $\frac{7\tau_p}{4}$, τ_p being the length of the 90° pulse. MSHOT3, with finite pulse lengths, eliminates dipolar terms of the Hamiltonian corresponding to irreducible tensor T_{2m} up to third order[29]. For finite bracketing pulses, the scale factor becomes $\frac{7\pi+8}{27\pi}$ relative to $\frac{1}{3}$ as calculated for sequences assuming δ-shaped 90° bracketing pulses[29].

Fig. 4 shows representative spectra of monoethyl fumarate obtained with the aforementioned sequences. Both TREV8 and MSHOT3 are z-rotation sequences which lead to relatively artifact-free and offset-independent spectra. The performance of these sequences is compared with the solid-echo based sequences like MREV8 and BR24.

2.3. *Lee-Goldburg based sequences*

When the sample is rotated physically along an axis which is $\theta_m = 54.7°$ inclined to the main magnetic field (B_0), spatial averaging is achieved for the anisotropic interactions. Similar averaging is achieved in the spin space by the Lee-Goldburg irradiation which provides averaging for the zero-order Hamiltonian. The irradiation is off-resonant, the value of which is given by $\Delta\omega = \omega_1 \arctan(\theta_m)$ where $\Delta\omega/2\pi$, $\omega_1/2\pi$, and θ_m represent the off-resonance value, RF amplitude, and the magic angle respectively. The duration of the pulse is

Figure 5: (a) Schematic of the LG irradiation as seen from the rotating frame of the RF. The amplitude ($\omega_1/2\pi$) and the offset ($\Delta\omega = \frac{\omega_1}{\sqrt{2}}$) of the RF irradiation result in creating an effective field tilted at an angle (θ_m), which does the averaging of the zero-order terms of the Hamiltonian in the spin space. (b) The FSLG pulse scheme and the time-dependent RF trajectory in the xy-plane of the on-resonance rotating frame. The offset frequencies $\Delta\omega/2\pi$ and $-\Delta\omega/2\pi$ obey the relation $\Delta\omega = \omega_1/\sqrt{2}$. The trajectory of $-\Delta\omega$ has been scaled down for the sake of clarity. (c) The schematic of the phase-modulated Lee Goldburg sequence, the phase modulation being shown on the left and the time-dependent RF trajectory in the xy-plane in the rotating on-resonance frame is shown on the right. The continuous time-dependent phase profile of the FSLG scheme is replaced by the PMLGn sequence of n discreet phases as shown in (c).

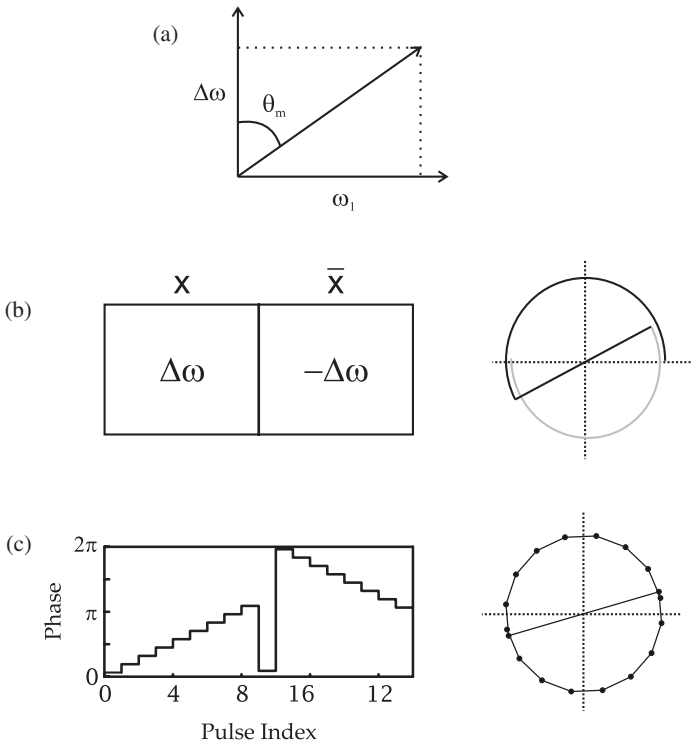

such that it creates a rotation of 360° for the resonant spins around the effective axis ($\tau_{LG} = \frac{2\pi}{\omega_{\text{eff}}}$) (Fig. 5a). The effective nutation frequency is given by $\omega_{\text{eff}} = \sqrt{\omega_1^2 + \Delta\omega^2}$. Although this sequence was one of the most pioneering work in the field of homonuclear decoupling and paved the way for the development of many schemes later, this in itself was not very useful in the sense that it only averages the homonuclear dipolar couplings to the zero order.

Symmetrisation of the sequence was required in order to eliminate the terms coming from the higher-order terms of the dipolar Hamiltonian. The first attempt in this direction came from Mehring and Waugh[42] where they switched the phase of the irradiation by a factor of π after each 2π rotation of the spins around the effective axis. The sequence was known as flip-flop Lee Goldburg (FFLG)[42]. This averages out the first-order correction terms to the Hamiltonian but the second order remains the same as that of the LG scheme. Whilst FFLG was implemented in the static case, the same was done in the spinning case by Bielecki et al.[43] by switching the phase by π as well as the carrier frequency from $+\Delta\omega/2\pi$ to $-\Delta\omega/2\pi$ after τ_{LG} duration (Fig. 5b). Both of these sequences had problems in implementation as they were demanding on the old hardware because of the requirement for the simultaneous switching of both the phase and the frequency.

A notable advance in this field came from Vinogradov et al. which involves on-resonant application of a series of pulses with discreet phases as described in Ref. [33]. The sequence is called phase-modulated Lee-Goldburg (PMLG) with the averaging of the zero- and first-order terms of the homonuclear dipolar interactions achieved by discreet modulation of the phases of the pulses. A PMLGn mimics an on-resonant LG irradiation by the application of n pulses of duration τ_{LG}/n ($n = 3, 5, 9$). The symmetrisation in this case was accomplished by repeating the same set of n pulses with the phases of the pulses shifted by 180°. A schematic of this sequence is given in Fig. 5c. A large number of developments ensued in this area of decoupling, with the analysis of the sequence using bimodal Floquet theory (BMFT)[54]. Initially this sequence was applied in a 2D ^{1}H $-^1$H spectroscopy with high-resolution spectra obtained in the indirect dimension. Later, windows were inserted which enabled the application of the sequence in a 1D fashion[55]. The windowed sequence is known as wPMLG. Great deal of understanding and development followed providing an insight into the role of imperfections in homonuclear decoupling[56]. A major improvement came with the introduction of a supercycling scheme which enabled on-resonant application of the sequence[34] as shown in Fig. 6.

Depending upon the phase values of the PMLG unit, the sequence is called PMLG$_p$ or PMLG$_m$ when the phase variation is clockwise or anticlockwise respectively. If the initial phase value falls in the first or fourth quadrant then the unit is named as PMLG^x whilst if it falls in the second or third quadrant it is called PMLG$^{\bar{x}}$. Following this nomenclature the PMLG unit shown in Fig. 5c is denoted as PMLG^x_m and the windowed supercycled scheme shown in Fig. 6 is denoted as wPMLG$^{\bar{x}x}_{mm}$.

Experimental implementation of the sequences PMLGn and wPMLG in various manners has been discussed in detail in Refs. [57,58]. We will mainly focus on the application of this sequence in the high spinning frequency regime.

Figure 6: (a) The schematic of the *w*PMLG$^{x\bar{x}}_{mm}$ sequence with A depicting the profile of the PMLG unit which is supercycled by 180° in consecutive steps. (b) A set of representative spectra of glycine obtained with *w*PMLG$^{x\bar{x}}_{mm}$ obtained on a 500 MHz spectrometer at a MAS frequency of 14 kHz spanning a range of 8 kHz in offset showing the on-resonance applicability of the sequence. The spectra were obtained with an RF field strength of 85 kHz. (Reproduced with permission from Ref. [67].)

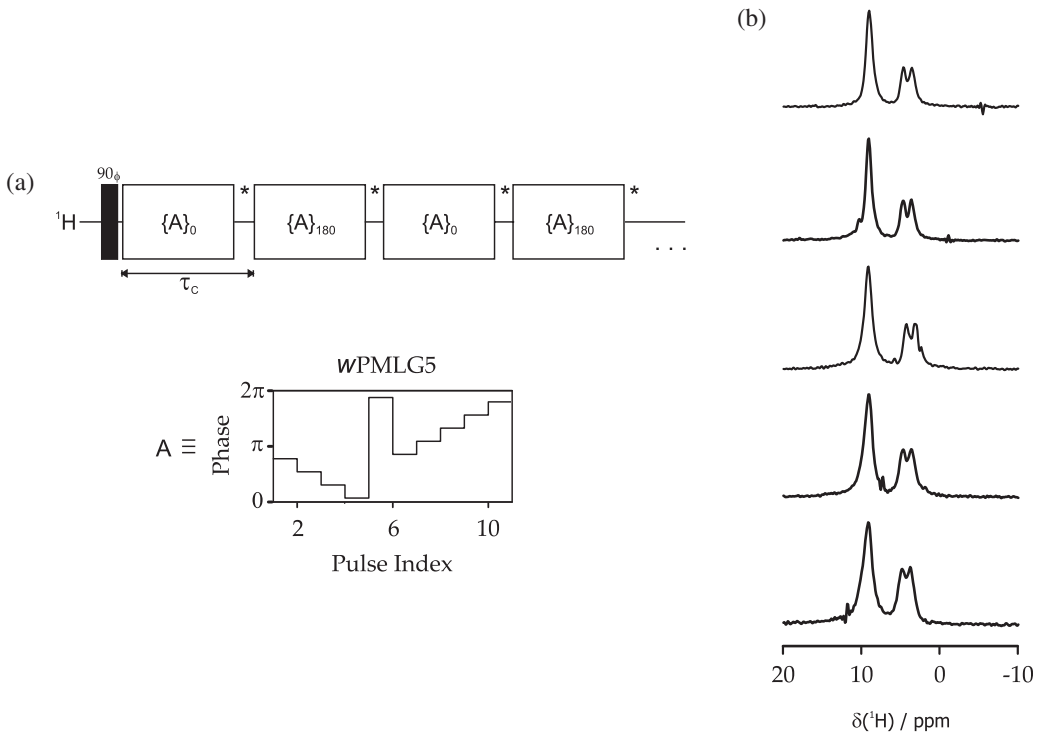

2.3.1. *PMLG in the high spinning frequency regime*

High MAS frequencies are required to study nuclei like ^{13}C and ^{31}P, that have large CSA values in high magnetic fields. ^{1}H being the most abundant nucleus in a molecule becomes very important for correlation experiments leading to structural characterisation. PMLG or *w*PMLG was initially applied at low spinning frequencies ($\omega_r/2\pi = \nu_r < 20$ kHz) and the common belief was that as the cycle time of the sequence (τ_c) becomes comparable to the rotation period (τ_r), the sequence may fail. Recently, it was shown that PMLG can work at high spinning frequencies also and has been successfully applied up to a spinning frequency of 65 kHz[46]. A theoretical description of why it should work is given in Ref. [47].

The Hamiltonians of the interactions depend on two characteristic frequencies, the cycle frequency of the sequence ($\omega_c/2\pi$) and the rotor frequency ($\omega_r/2\pi$). These two frequencies are not necessarily commensurate. AHT cannot deal with two such incommensurate frequencies. Hence, to appreciate the success of PMLG we have to rely on the bimodal Floquet theory which allows us to derive an effective Hamiltonian for a spin system experiencing two time dependences simultaneously. The time-dependent Floquet Hamiltonian in the Fourier space can be represented as[50]:

$$\mathcal{H}^F_{\text{int}}(t) = \sum_{n,k} \mathcal{H}_{n,k} F^r_n F^c_k \exp^{in\omega_r t} \exp^{ik\omega_c t} \qquad (5)$$

where $\mathcal{H}_{n,k}$ are infinite dimensional matrices and F's are the ladder operators[59]. A complete representation of these operators is given in Ref. [50]. The problem still remains that the matrix elements are time dependent in nature. To make these Hamiltonians time independent we make a similarity transformation using an operator known as the number operator, N[59]. The transformation is shown as follows:

$$\exp^{-iN^c\omega t_c} \exp^{-iN^r\omega t_r} \mathcal{H}^F_{\text{int}} \exp^{iN^r\omega t_r} \times \exp^{iN^c\omega t_c} = \sum_{n,k} \mathcal{H}_{nk} + \omega_r N^r + \omega_c N^c$$

$$\mathcal{H}_{nk} = \sum_{n,k} \mathcal{H}^{CS}_{nk} + \mathcal{H}^{DD}_{nk} \qquad (6)$$

Figure 7: The position of the (a) zero-order and (b) first-order degeneracy plotted as a function of ψ. Here k was $-15 \geq k \geq 1$ for both the cases. The sparse recoupling conditions at high ψ values favour experimental setup in those regions.

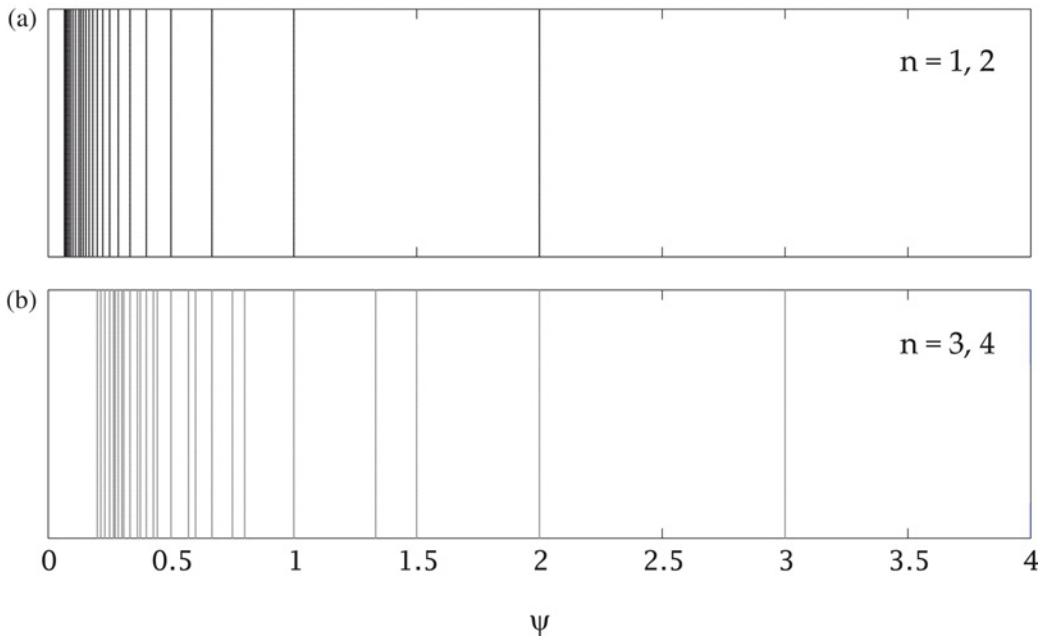

We consider only the isotropic chemical shift and heteronuclear dipolar couplings in Eq. (6) whilst the other interactions including the CSA of the protons can be ignored owing to their small magnitude. The chemical shift and dipolar Hamiltonian can be represented as:

$$\mathcal{H}_{nk}^{CS} = \sum_{m,a} \Delta\omega_a d_{m,k}^{(1)} T_{m,a}^{(1)} F_0^r F_k^c$$

$$\mathcal{H}_{nk}^{DD} = \sum_{m,a<b} \omega_{ab} G_n^{ab} d_{m,k}^{(2)} T_{m,a}^{(2)} F_n^r F_k^c \quad (7)$$

where $\Delta\omega_a$ is the isotropic chemical shift for spin a. The geometric dependence of the dipolar couplings between the spins a and b with characteristic frequency ω_{ab} is given by the G_n coefficients ($n = \pm 1, 2$) with the spin part of the chemical-shift and dipolar interactions defined by the irreducible tensor operators $T_m^{(l)}$[50]. The most important terms in Eq. (7) are the Fourier coefficients $d_{m,k}^{(l)}$ which determine the quality of the decoupling sequence. These coefficients are dependent on the experimental parameters such as the RF amplitude $\omega_1/2\pi$, cycle frequency of the pulse sequence $\omega_c/2\pi$, and RF imperfections of the pulse sequence. These dependencies have been described in detail in Ref. [50].

To understand the decoupling performance and the feasibility of the application of these sequences at high spinning frequencies, we have to derive an effective Hamiltonian. For chemical-shift interactions the approximation up to zero order is sufficient. The zero-order Hamiltonian for the chemical shift can be written as:

$$\widetilde{\mathcal{H}}_{00}^{CS(0)} = \sum_{m,a} \Delta\omega_a d_{m,0}^{(1)} T_{m,a}^{(1)} F_0^r F_0^c \quad (8)$$

The magnitude by which the chemical shift is scaled is given by:

$$s = \sqrt{|d_{-1,0}^{(1)}|^2 + |d_{0,0}^{(1)}|^2 + |d_{1,0}^{(1)}|^2} \quad (9)$$

where s is the scaling factor. The Fourier coefficients define the direction of the effective field and also the scaling factor which should be maximised to increase the spread of the chemical shift.

In order to derive the effective Hamiltonian for the dipolar couplings, we have to diagonalise the Floquet Hamiltonian. For that we need to perform a van Vleck transformation[60], keeping in mind certain synchronisation conditions between the cycle frequency and the MAS frequency which give us the notion that high RF frequencies are necessary to work at high MAS frequencies.

Figure 8: (I) The magnitude of the χ parameter plotted as a function of the RF amplitude $\omega_1/2\pi$ and ψ for wPMLG$^{x\bar{x}}_{mm}$ for cycle times (a) 20 kHz, (b) 30 kHz, (c) 40 kHz, and (d) 50 kHz. The top axis shows specific spinning frequencies in kHz. The χ parameter cannot be used to evaluate the decoupling efficiency near the degeneracy regime. (II) shows the cuts from the four contours of (I). (IIa) reveals that there is not much decrease in the line width as we go to the high spinning frequencies but (IIb) reveals that the width of the degeneracy bands narrows down as we go from 20 kHz spinning frequency to 50 kHz spinning frequency making it feasible to work at high spinning frequency as described in the text. (Reproduced with permission from Ref. [47].)

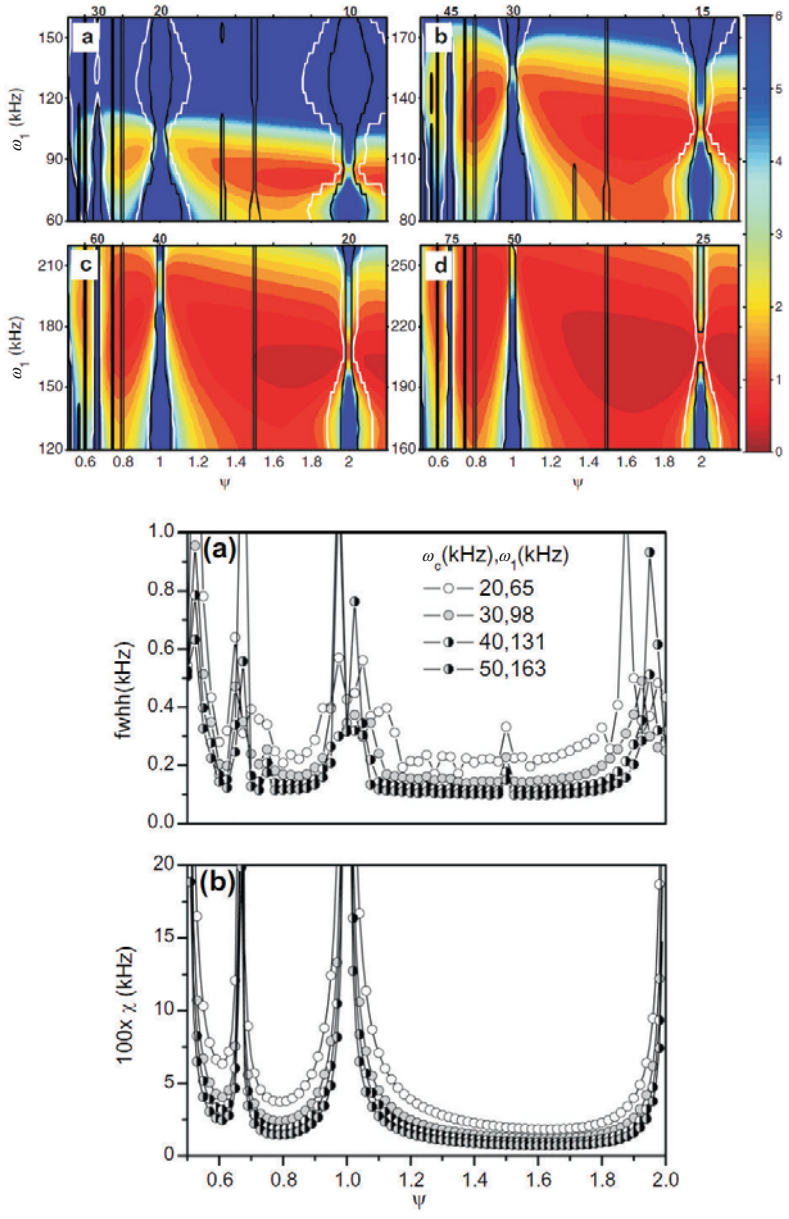

1. $k\omega_c = \omega_r$ *or* $2\omega_r$: This synchronisation leads to degeneracies between the elements with $n = 1, 2; k$ and the zero-order off-diagonal elements become significantly large[50,61]. In this situation van Vleck transformation cannot be performed and direct diagonalisation is the only way. This condition is known as the zeroth-order degeneracy condition and it leads to severe line broadening.
2. $k\omega_c = 3\omega_r$ *or* $4\omega_r$: In this case van Vleck transformation can be done, but the diagonal blocks of $(n = 3, 4; k)$ are connected by

elements formed by the first-order van Vleck transformation. This condition is known as the first-order degeneracy condition and it leads to the presence of artifacts in the spectra known as rotor-radio-frequency (RRF) lines. If these lines fall on the spectra, they lead to line broadening[50,61].

3. $k\omega_c = n\omega_r (n > 4)$: In this case the degenaracy between the diagonal blocks is not reflected in the first order of approximation, as the degenerate diagonal blocks are not connected by off-diagonal dipolar elements up to the first order[50,61].

Considering $n = 1, 2, 3, 4$ and $-15 \leq k \leq -1$, we plot the different recoupling conditions as a function of ψ where, $\psi = \frac{\omega_c}{\omega_r}$ (Fig. 7). From the plot (Fig. 7) it can be seen that with the increasing ψ value the recoupling conditions become sparse. Hence, it is safe to work at high ψ values. This implies that given a MAS frequency $\omega_r/2\pi$, we have to increase the value of ω_c to work in a region with sparse recoupling conditions. Hence, we have to decrease the length of the pulses and thereby increase the RF amplitude for the overall pulse sequence as we increase the spinning frequency.

Avoiding the zero-order degeneracy condition we can apply the van Vleck transformation to derive a first-order Hamiltonian for the dipolar couplings which can be written as:

$$\widetilde{\mathcal{H}}_{nk}^{DD(1)} = -1/2 \sum_{m,n,a<b,b<c} \omega_{ab}\omega_{bc} G_n^{ab} G_{-n}^{ab} \times \Delta_{m,m'}^{n,k} [T_{m,ab}^{(2)}, T_{m',bc}^{(2)}] F_n^r F_n^c \quad (10)$$

where,

$$\Delta_{m,m'}^{n',k} = \sum_{k'} \frac{d_{m,k}^{(2)} d_{m',-k}^{(2)}}{\omega_r (n + k\psi)} \quad (11)$$

When there is no synchronisation between the MAS frequency and the cycle frequency Eq. (11) is the main source of line broadening. To achieve good decoupling we have to minimise the Δ parameter. Another factor that has to be kept in mind is that with the increase in the RF amplitude the scaling factor also decreases. A parameter has to be defined which would take into account the Δ value as well as the scaling factor (s) justifying the decoupling performance of the sequence. Such a parameter χ^2 was defined in Ref. [47] as follows:

$$\chi^2 = \frac{\sum_{n,m \geq m'} |\Delta_{m,m'}^{n0}|^2}{\sum_{m''} |d_{m'',0}^{(1)}|^2} \quad (12)$$

χ being dependent on the Fourier coefficients will change according to the RF parameters and the spinning frequency, and thus will be a reliable parameter in evaluating the performance of a sequence provided we do not work in the vicinity of a degeneracy condition where $n + k\psi \longrightarrow 0$ and the parameter becomes undefined.

Close inspection of this parameter χ reveals that with the increase in the spinning frequency, the width of the degeneracy bands narrows down. To explain this calculations are shown in Fig. 8. If we increase the spinning frequency and examine the region near the $\psi = 1$ condition, it is observed that at low spinning frequency the region around the $n = 1$ degeneracy condition is much broader compared to the region around the same at higher spinning frequency. To work at high spinning frequency at optimal RF power ($\omega_1/2\pi < 250$ kHz) we have to work near the $n = 1$ or $n = 2$ condition and avoiding the degeneracy region becomes important. From Fig. 8(Id) it becomes clear that at high spinning frequency such as 50 kHz it is feasible to work around a cycle time of 50 μs as the degeneracy condition becomes narrow and we do not need low cycle times as was the popular belief for "quasi-static" approximation. The decrease in the width of the degeneracy band helps in that sense, though the overall decoupling performance does not improve as reflected by the magnitude of the χ parameter. A spectrum of L-tyrosine.HCl obtained at 65 kHz of spinning frequency is compared with the same obtained at 10 kHz in Fig. 9. The spectrum obtained at 10 kHz was acquired with $\psi = 2.65$ whilst the same for 65 kHz was 0.63.

To conclude, it is possible to combine PMLG with ultra-fast spinning frequencies, owing to narrowing of regimes around the degeneracy conditions. Ultra-fast MAS frequencies may not provide much gain in the resolution of the spectra, but makes it very convenient for hetero-correlation experiments where the protons can be correlated to nuclei of high CSA.

2.4. *Symmetry based sequences*

In this section we review the progress in the field of homonuclear decoupling utilising symmetry based rotor-synchronised sequences. Symmetry sequences were designed by Levitt[44] to select certain desired interactions whilst filtering out the other interactions based on the differences in the rotational properties of these interactions in the co-ordinate space and the spin space. The rotational ranks of the spin interactions are given in Table 1. Here we focus on three sequences CN_n^ν, RN_n^ν, and the recently introduced SAM or wSAM scheme[31].

Figure 9: ^{1}H spectra of L-tyrosine.HCl.H_2O obtained with wPMLG$^{x\bar{x}}_{mm}$ at (a) 65 kHz and (b) 10 kHz of MAS frequency. The spectra at 10 kHz was acquired with $\psi = 2.75$ whilst that at 65 kHz was acquired with $\psi = 0.63$ which indicates that it is possible to obtain a well-resolved spectra at ψ values less than 1. (Reproduced with permission from Ref. [46].)

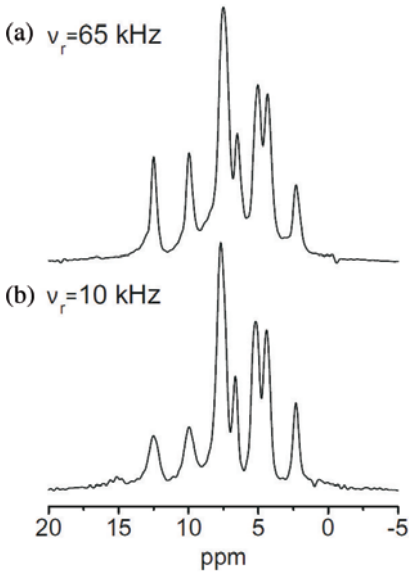

2.4.1. CN^{ν}_{n} sequences

The CN^{ν}_{n} sequence has n number of rotor periods divided into N intervals, each of which performs a 2π rotation of the spins. Each element is phase shifted by $\phi = \frac{2\pi\nu}{N}$. The basic construction of the sequence is shown in Fig. 10a. N and ν are known as spin-winding and space-winding numbers. The selection rules for the selection of interactions have been theoretically derived by both AHT[44] and single-mode Floquet theory which deals with a single characteristic frequency as the MAS frequency and the cycle frequency of the symmetry sequences are commensurate[50]. Since we are dealing with the selection of the isotopic chemical-shift interactions, we will restrict ourselves to the zero-order selection rule. The higher-order selection rules have been described thoroughly in Ref. [44] and hence not described here. The zero-order selection rule can be written as:

$$\widetilde{\mathcal{H}}^{(0)}_{lm\lambda\mu} = 0 \text{ if } mn - \mu\nu \neq NZ \tag{13}$$

where l and λ are the space rank and the spin rank, respectively, whilst m are the components of the space rank and μ are the components of the spin rank. m can have values $-l, -l+1, \ldots, l$ and μ can have values $-\lambda, -\lambda+1, \ldots, \lambda$. Here Z is an integer.

If we work out the inequality then it becomes evident that sequences like $C4^0_1$ allow the $\mu = 0$ component of the isotropic chemical shift for $Z = 0$. Homonuclear dipolar terms having $l = 2$ and $\lambda = 2$ are all symmetry forbidden. The scaling factor of these sequences is however zero making them inappropriate for high-resolution ^{1}H spectroscopy.

2.4.2. RN^{ν}_{n} Sequences

The RN^{ν}_{n} sequence is another class of rotor-synchronised sequence developed by the group of Levitt and has been used for high-resolution ^{1}H spectroscopy.[44,63]. Here n rotor periods are divided into $N/2$ intervals comprising of $[R_\phi R'_{-\phi}]$ elements. Each R_ϕ element creates a 180^o rotation of the spins and the phase ϕ is defined by $\phi = \frac{\pi\nu}{N}$. The basic construction is shown in Fig. 10b. The selection rule derived by AHT[44] or single-mode Floquet theory[50] is as follows:

$$\widetilde{\mathcal{H}}^{(0)}_{lm\lambda\mu} \neq 0 \text{ if } mn - \mu\nu = \frac{N}{2} Z_\lambda \tag{14}$$

Z_λ indicates that Z depends on the parity of λ. So if the spin rank is even Z takes the values $0, \pm 2, \pm 4, \ldots$ whilst an odd rank of λ implies that Z takes the values $\pm 1, \pm 3, \pm 5, \ldots$.

Let us consider an R-sequence of the nature $RN^{N/2}_{n}$. The selection rule can be written as:

$$mn = (\mu + Z_\lambda)\frac{N}{2} \tag{15}$$

For isotropic chemical shift the space rank is always 0 ($l = 0 \Rightarrow m = 0$) and hence Eq. (15) can be written as:

Table 1: Spin and space ranks of homonuclear spin interactions in the case of exact magic-angle spinning.

Interaction	Space Rank (l)	Space Components (m)	Spin Rank (λ)	Spin Components (μ)
Isotropic chemical shift	0	0	1	1, 0, −1
J couplings	0	0	0	0
Dipolar couplings	2	−2, −1, 0, 1, 2	2	−2, −1, 0, 1, 2
Chemical shift anisotropy	2	−2, −1, 0, 1, 2	1	−1, 0, 1

Figure 10: Construction principle of the CN_n^ν and the RN_n^ν sequences.

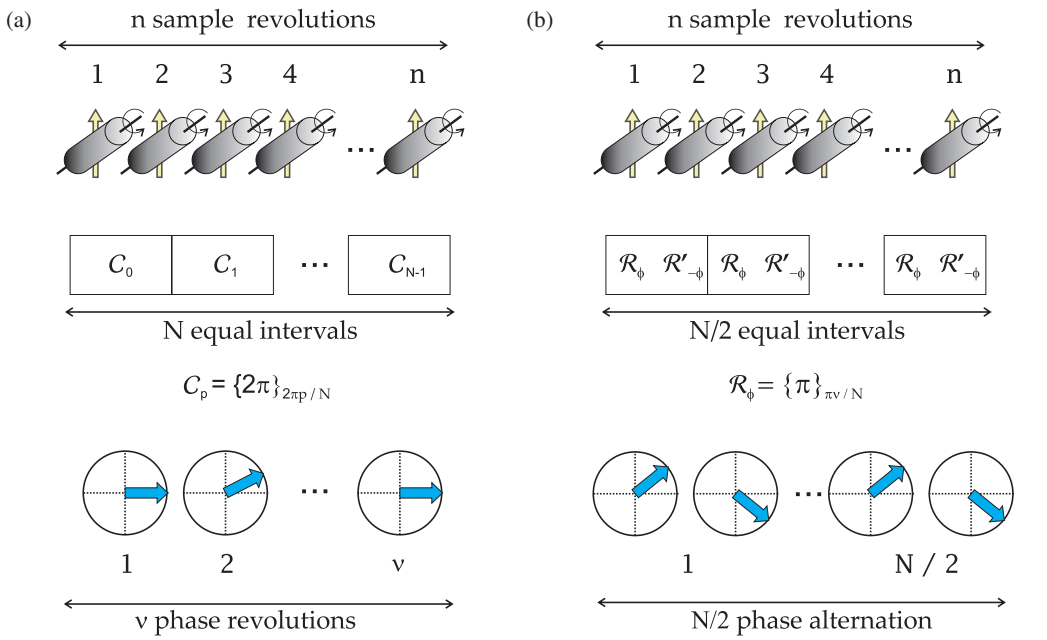

$$(\mu + Z_\lambda)\frac{N}{2} = 0$$
$$\Rightarrow \mu = -Z_\lambda \qquad (16)$$

For isotropic chemical shift $\mu = \pm 1, 0$ whilst Z_λ following the parity of λ which is odd here can take values $Z_\lambda = \pm 1, \pm 3, \pm 5, \ldots$. So we can see from Eq. (16) that the terms $(0, 0, 1, \pm 1)$ are filtered out. Thus $RN_n^{N/2}$ sequences are suitable for selecting isotropic chemical shift and also the scalar J-coupling having $(0, 0, 0, 0)$ as the space and spin rank. Let us consider such a sequence $R8_1^4$ here and look at the the DD and CSA couplings. The DD coupling has terms like $(2, m, 2, \mu)$. Considering one of the terms like $(2, 1, 2, -1)$ and putting it into Eq. (15) it can be seen that $mn = 1$ whilst $(\mu + Z_\lambda)\frac{N}{2}$ assumes the value $(-1 + (0, \pm 2, \pm 4, \ldots)\ 4)$. So Eq. (15) is never satisfied. Similarly all the terms are filtered out for the DD couplings except the $(2, 0, 2, 0)$ which is anyway averaged out under MAS. The CSA has terms like $(2, m, 1, \mu)$. Considering one of the terms like $(2, 1, 1, 1)$ and putting it into Eq. (15), it can be seen that $mn = 1$ whilst the right-hand side of the equation assumes the values $(1 + (\pm 1, \pm 3, \ldots)\ 4)$ and as a result Eq. (15) is never satisfied and the CSA interactions are blocked. R-sequences with ($N \leq 20$, $n \leq 10$, and $\nu \leq 10$) are listed in Table 2.

Table 2: RN_n^ν symmetries for the observation of isotropic chemical shifts and heteronuclear J couplings under MAS. All the mentioned RN_n^ν sequences select isotropic chemical-shift terms (l, m, λ, μ) = (0,0,1,±1). All the CSA and homonuclear DD coupling terms are suppressed. The inequivalent terms in the range of $N \leq 20$, $n \leq 10$ and $\nu \leq 10$ are shown in the table.

$n = 1$	$R6_1^3\ R8_1^4\ R10_1^5\ R12_1^6\ R14_1^7\ R16_1^8\ R18_1^9\ R20_1^{10}$
$n = 2$	$R6_2^3\ R10_2^5\ R14_2^7\ R18_2^9$
$n = 3$	$R8_3^4\ R10_3^5\ R14_3^7\ R16_3^8\ R20_3^{10}$
$n = 4$	$R6_4^3\ R10_4^5\ R14_4^7\ R18_4^9$
$n = 5$	$R6_5^3\ R8_5^4\ R12_5^6\ R14_5^7\ R16_5^8\ R18_5^9$

R-sequence was first applied to observe J-coupling in adamantane and in the high-resolution spectroscopy of protons on a sample of alanine and monoethyl fumarate[63]. $R18_2^9$ was used for this purpose and it was seen that the performance becomes much superior when the basic unit comprises of a composite 180° pulse. The RN_n^ν sequence was based on $R_\phi = 90_{45}90_{-45}90_{45}$ and $R'_{-\phi} = 90_{45}90_{-45}90_{45}$. For high-resolution proton spectroscopy the R-sequence was applied in a 2D manner with the indirect dimension yielding high-resolution ^{1}H spectra. A schematic of the pulse sequence is shown in Fig. 11a. Similar experiments were carried out later on samples of alanine and glycine at MAS frequencies of 20 kHz, 25 kHz, and 30 kHz, the results of which

Figure 11: (a) Pulse sequence employing RN_n^ν sequence to observe ^{1}H chemical shifts. Some of the RN_n^ν sequences suitable to filter out isotropic chemical shifts are given in Table 2. The phases of the 90° pulses are indicated on top of the pulses where ϕ on the final 90° pulse indicates a phase cycling of $[x, y, \bar{x}, \bar{y}]$. The R block is of the type $[180^\circ_{90}180^\circ_{-90}]$ where the 180°_{90} is substituted with a composite pulse of $90^\circ_{45}90^\circ_{135}90^\circ_{45}$ for better off-resonance behavior. (b–d) ^{1}H L-alanine spectra obtained with the pulse sequence in Fig. 11a. Also shown are alanine MAS spectra at 20 kHz, 25 kHz, and 30 kHz on the left and high-resolution ^{1}H spectra using $R6_1^3$, $R16_3^8$, and $R10_2^5$ respectively on the right which are the skyline projections of the indirect dimension of 2D spectra. (e–f) ^{1}H glycine spectra obtained with the pulse sequence in Fig. 1a. Also shown are glycine MAS spectra at 25 kHz and 30 kHz on the left and high-resolution ^{1}H spectra using $R16_3^8$ and $R10_2^5$ respectively on the right which are the skyline projections of the indirect dimension of 2D spectra. The RF power applied are listed in Table 3. (Reproduced with permission from Ref. [30].)

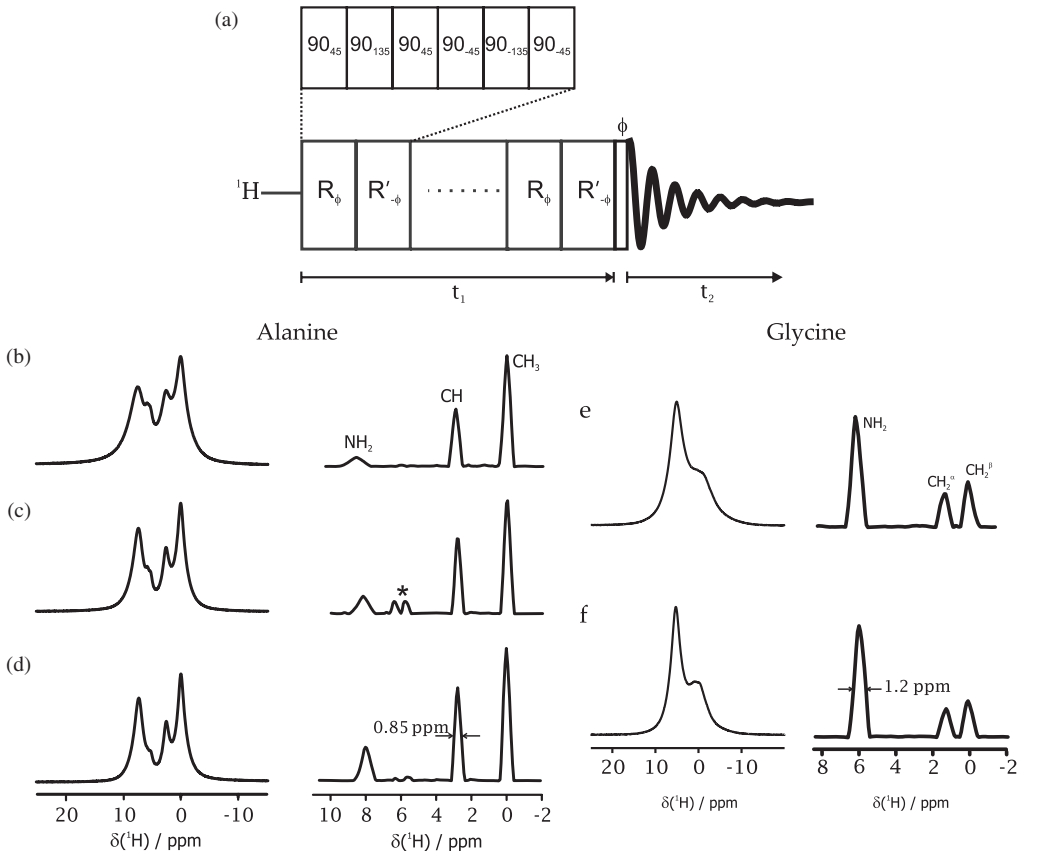

are shown in Fig. 11b–11f[30]. The R-sequence used were $R6_1^3$, $R16_3^8$, and $R10_2^5$ respectively. The left panel of the corresponding spectra obtained with a single 90° pulse whilst the right panel shows the skyline projection of the indirect dimension. The resolved CH_2 peak of glycine gives ample evidence of the potential of the R-sequence in the field of homonuclear decoupling. Since the basic element R_ϕ is composed of three 90° pulses or an effective 270° rotation of the spin-system, the RF power requirement is $\omega_1 = \frac{3}{4}\frac{N}{n}\omega_r$. These sequences have a high offset dependence and the optimum experimental offset is found to be around $-10(\pm 2)$ kHz and +7 (± 2) kHz.

Fig. 12 shows simulations done at high spinning frequencies of 40 kHz, 50 kHz, and 60 kHz with R sequences $R10_3^5$, $R16_5^8$, and $R16_5^8$ respectively. The simulations were done using SPINEVOLUTION[64] on a four spin system with dipolar coupling of -27 kHz (between spins 1 and 2), -22 kHz (3 and 4), -9 kHz (1 and 3), -7 kHz (2 and 3), -7 kHz (1 and 4), and -5 kHz (2 and 4). The simulation results show that at moderate power of 100 kHz -150 kHz, it is possible to obtain high-resolution ^{1}H spectra at high spinning frequencies whilst the same for PMLG or DUMBO was much higher[46,30]. The RF power requirement for the sequences applied are listed in Table 3.

Table 3: A table of RN_n^ν sequences used to obtain high-resolution ^{1}H spectra shown in Figs. 11 and 12. The MAS frequency and the RF field required are given for the various RN_n^ν sequences having the composite pulse scheme of $90^o_{45}90^o_{135}90^o_{45}$ as the basic R-element.

RN_n^ν sequences	MAS frequency ($\omega_r/2\pi$ in kHz)	RF field (ω_{nut} as a multiple of ω_r)	RF field needed ($\omega_{nut}/2\pi$ in kHz)
$R6_1^3$	20	$4.5\omega_r$	90.0
$R16_3^8$	25	$4.0\omega_r$	100.0
$R10_2^5$	30	$3.75\omega_r$	112.5
$R10_3^5$	40	$2.5\omega_r$	100.0
$R16_5^8$	50	$2.4\omega_r$	120.0
$R16_5^8$	60	$2.4\omega_r$	144.0
$R16_3^8$	30	$4.0\omega_r$	120.0

Figure 12: Simulated ^{1}H spectra of a four-spin system with dipolar coupling of 27 kHz, 22kHz, 10 kHz, 7 kHz, 7 kHz, and 4 kHz. The simulations were done at MAS frequencies of (a) 40 kHz, (b) 50 kHz, and (c) 60 kHz using R sequences $R10_5^3$, $R16_5^8$, and $R16_5^8$, respectively. The nutation RF required for the three sequences at the aforementioned MAS frequencies are 100 kHz, 120 kHz, and 144 kHz (Table 3). The chemical shift was scaled by a scaling factor of 0.59. The simulations were performed using the ZCW scheme of powder averaging[68–70] with 233 pairs of crystallite orientations. (Reproduced with permission from Ref. [30].)

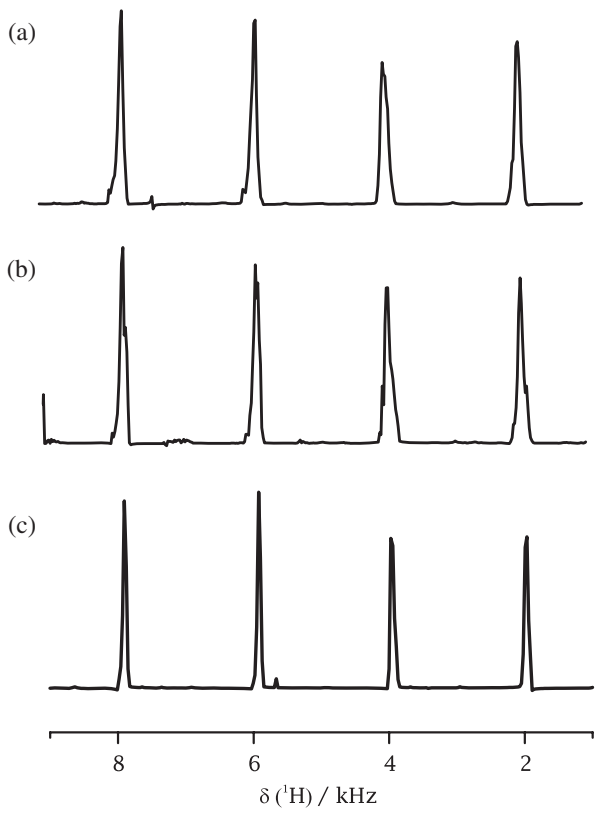

2.4.3. *SAM sequence*

This sequence is actually a subclass of the aforementioned sequences. The authors claim it to be a subclass of $CN_n^{N/2}$ sequence[31,48,49]. The basic element of a CN_n^ν sequence induces a 360° rotation of the spin-system. 2π rotation basic elements scale the chemical shift to zero. Hence, the CN_n^ν sequences are not suitable for ^{1}H high-resolution spectroscopy. The modification that was done to the $CN_n^{N/2}$ sequence was that instead of using a 2π basic element, a basic element was used consisting of two identical pulses which induces α^o rotation with alternating phases of $\pm x$. The basic element is repeated $N-1$ times and is sandwiched between two further α pulses, all with alternating phases as shown in Fig. 13a–13b. In order to avoid pulse transients the overall unit was replaced by a rotor-synchronised cosine modulation of amplitude. The amplitude in the time domain follows the function[48]:

$$\omega_1(t) = \omega_1^{\max}\cos\left(\frac{N}{2n}\omega_r t\right) \tag{17}$$

where $\omega_1^{max}/2\pi$ and $\omega_r/2\pi$ denote the maximum value of the RF nutation frequency and the MAS frequency, respectively. This sequence was called $\mathrm{SAM}_{N/2n}$[48] and is renamed as $CN_n^{N/2}$ (half-cos)[49]. For the sake of clarity the sequences will be referred to as $\mathrm{SAM}_{N/2n}$ here.

The scaling factor of these sequences is given by[49]:

$$\begin{aligned}\kappa_{0,0,1,0} &= \mathrm{sinc}(\alpha) \text{ for } CN_n^{N/2}(\alpha_x\alpha_{\bar{x}})\\ \kappa_{0,0,1,0} &= J_0(2\alpha/\pi) \text{ for } SAM_{N/2n}\end{aligned} \tag{18}$$

where $\mathrm{sinc}(\alpha) = \sin(\alpha)/\alpha$, and J_0 is the zero-order Bessel function.

The optimum RF power required for these sequences was obtained with simulations using SIMPSON[65] and was found to be[49]:

$$\begin{aligned}\omega_1 &= N\omega_r/2n \text{ for } CN_n^{N/2}(\alpha_x\alpha_{\bar{x}})\\ \omega_1 &= 1.15N\omega_r/2n \text{ for } SAM_{N/2n}\end{aligned} \tag{19}$$

The angle α is defined in radians as[49]:

$$\alpha = \pi\frac{n\omega_1^{max}}{N\omega_r} \tag{20}$$

Windows were inserted to implement these sequences in a 1D fashion[48], the length of which was adjusted in such a fashion so that the dipolar interaction gets averaged out after a certain number of acquisition points. The windowed experiments require higher power compared to the windowless

Figure 13: (a) Schematics of $CN_n^{N/2}$ sequence and SAM sequence with C_0C_π as the basic unit. (b) Schematics of the windowed acquisition implementing the aforementioned sequences. (c–e) ^{1}H spectra of glycine obtained with 31.746 kHz of MAS frequency by applying (c) single excitation pulse (d) $C14_2^7$, and (e) $SAM_{3.5}$ in the indirect dimension whilst acquisition under MAS in a ^{1}H –^{1}H correlation spectroscopy. For (d–e) the maximum RF power applied was 103 kHz and 120 kHz respectively. (Reproduced with permission from Ref. [49].)

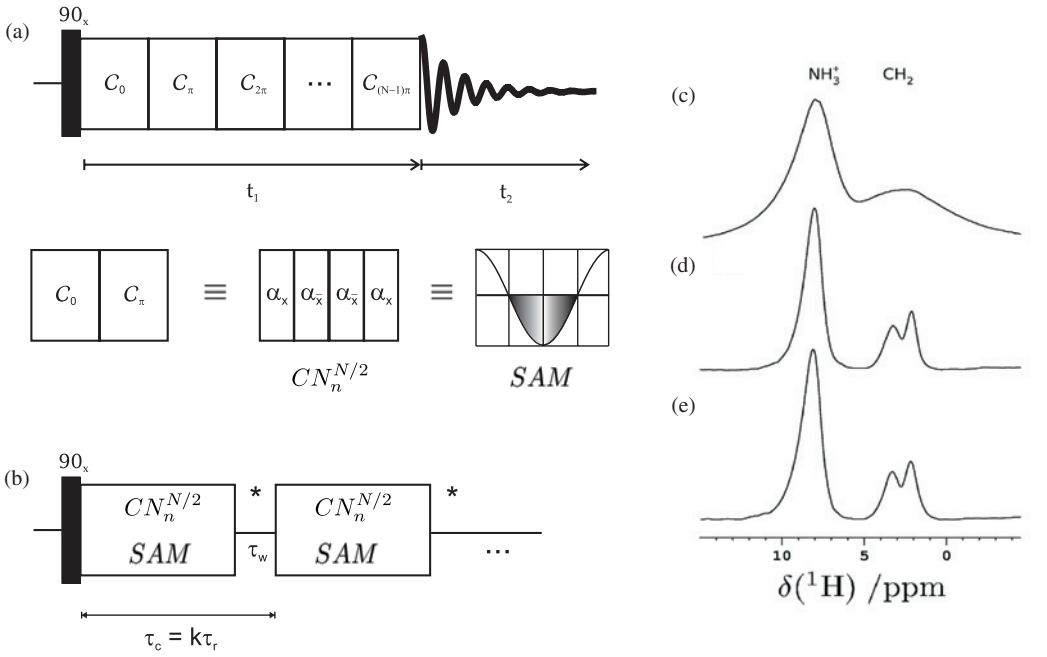

experiments which seems to be reasonable for the compensation of the acquisition windows. Further it was also found out that the best resolution is obtained when $\frac{N}{2n} = 3$ or $\frac{N}{2n} = 3.5$. The scale factor of 0.69 was calculated by using a sample of adamantane and found to be consistent over the spectrum. It was observed that severe line broadening occurs in the offset range of -4 kHz to $+1$ kHz[49]. This can be analysed in terms of Floquet theory in the same fashion as PMLG sequence. The position of the RRF lines are given by

$$\Delta N = n'\omega_r + k\omega_c \tag{21}$$

In order to distinguish from the notation used for the symmetry sequences, we denote n of Eq. (11) as n' here.

Let us consider the zero-order degeneracy condition at $\Delta N = 0$ where $\omega_r = k\omega_c$ or $2\omega_r = k\omega_c$ with $(-\infty \geq k \geq \infty)$. For a $CN_n^{N/2}$ sequence:

$$\begin{aligned} \omega_c &= \frac{N\omega_r}{2n} \\ \Rightarrow k &= \frac{2n}{N} \text{ when } n' = 1 \\ \text{or } k &= \frac{4n}{N} \text{ when } n' = 2 \end{aligned} \tag{22}$$

For all the $CN_n^{N/2}$ sequences the above condition gets satisfied and hence line broadening is observed around the region of $\Delta N = 0$.

Fig. 13c–13e shows spectra of glycine obtained at 31.746 kHz MAS frequency using $C14_2^7(\alpha_x\alpha_{\bar{x}})$ and $SAM_{3.5}$ and compared with the same obtained under MAS alone.

2.5. *DUMBO at high spinning frequencies*

The DUMBO group of homonuclear decoupling scheme consists of a continuous phase-modulated RF irradiation of constant amplitude given by[66]:

$$\mathcal{H}_{rf}(t) = \omega_1[I_x\cos\phi(t) + I_y\sin\phi(t)] \tag{23}$$

where $\omega_1/2\pi$ denotes the constant amplitude and the periodic phase modulation is defined by a Fourier series[32]:

$$\begin{aligned} \phi(t) = \sum_{n=1}^{6}\Bigg[& a_n\cos\left(\frac{4n\pi t}{\tau_c}\right) \\ & + b_n\sin\left(\frac{4n\pi t}{\tau_c}\right)\Bigg] \text{ if } 0 \leq t < \tau_c/2 \\ \phi(t) = \pi + \phi(\tau_c - t) & \text{ if } \tau_c/2 \leq t < \tau_c \end{aligned} \tag{24}$$

Figure 14: Spectra of β-L-Asp-L-Ala obtained with a spinning frequency of 65 kHz. (a) Spectrum obtained by a single pulse excitation and (b) spectrum obtained by implementing eDUMBO-1_{22} in a windowed fashion. The arrow indicates the position of the carrier frequency. (Reproduced with permission from Ref. [45].)

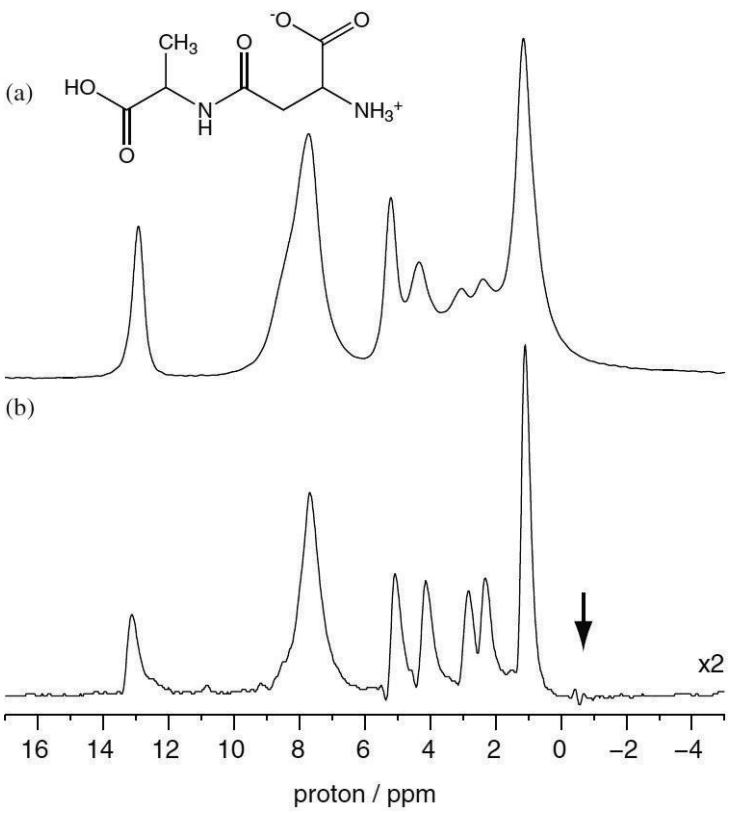

where τ_c denotes the overall cycle time of the sequence. The sequence gives a good decoupling performance when τ_c is approximately equal to the length of a 6π pulse[32]. a_n and b_n are the Fourier coefficients which define the phases of the sequence. There are two classes of DUMBO sequence, DUMBO-1[32] and eDUMBO-1[66]. These two classes of sequence differ in the way the Fourier coefficients in Eq. (24) are optimised. For DUMBO-1 these coefficients were derived by numerical optimisation and the number of phases per cycle was kept at 64 so that it can be applied by using the commonly available experimental hardwares[32]. In the case of eDUMBO-1, the coefficients were optimised experimentally starting from the values obtained by numerical optimisation of DUMBO-1. The optimisation was done by monitoring the resolution of the ^1J doublet of the CH peak of L-alanine[66].

Both of these sequences have been applied at a spinning frequency of 65 kHz[45]. The sequences were implemented in 2D ^{1}H $-^1$H correlation spectroscopy with the DUMBO sequence in the indirect dimension and acquisition under MAS in the direct dimension. They were also applied in 1D manner with acquisition windows. When windowed DUMBO was applied, three repetitive DUMBO blocks of $\tau_c = 20\mu s$ each were separated by a detection window of 7.6 μs[45]. The sequences were applied on a sample of glycine and a dipeptide β-L-Asp-L-Ala. A representative spectra of the dipeptide obtained at 65 kHz of MAS frequency using the windowed eDUMBO-1 is shown in Fig. 14. The eDUMBO-1 has a scaling factor of 0.55 whilst that for the DUMBO-1 sequence is 0.47[45]. The sequence has been successfully applied for a series of spinning frequencies from 20 kHz to 65 kHz. A gain in intensity was observed at higher spinning frequencies but there was no gain in terms of resolution[45].

3. Conclusion

We have presented here an overview of homonuclear decoupling sequences at moderate to ultra-fast spinning frequencies. It has been observed that the symmetry sequence (RN_n^ν) has the potential to deliver higher resolution than the previously reported sequences up to spinning frequency of 30 kHz, above which it has not been implemented yet. At ultra-fast spinning frequencies (65 kHz) PMLG and DUMBO give comparable performance.

Acknowledgements

We acknowledge the use of the Bruker AV 500 MHz spectrometer in the National Facility for High Field NMR, TIFR, and technical assistance of M. V. Naik.

Received 02 November 2009; accepted 05 November 2009.

References

1. M. J. Duer, 'Introduction to solid-state NMR spectroscopy', Blackwell Science, UK, (2002).
2. M. Etzkorn, S. Martell, O. C. Andronesi, K. Seidel, M. Engelhard, M. Baldus, 'Secondary structure, dynamics, and topology of a seven-helix receptor in native membranes, studied by solid-state NMR spectroscopy', *Angew. Chem.* 46, 3, pp. 309–473, (2007).
3. R. Tycko, 'Applications of solid state NMR to the structural characterization of amyloid Fibrils: Methods and results', *Prog. Nucl. Magn. Reson. Spectrosc.* 42, 1–2, pp. 53–68, (2003).
4. R. Tycko, 'Progress towards a molecular-level structural understanding of amyloid fibrils', *Curr. Opin. Struct. Biol.* 14, 1, pp. 96–103, (2004).
5. K. J. D. Mackenzie, M. E. Smith, 'Multinuclear solid-state nuclear magnetic resonance of inorganic materials' (Pergamon Material Science) Pergamon Press, Oxford, (2001).
6. K. Schimdt-Rohr, H. W. Speiss, 'Multidimensional solid-state NMR and polymers', Academic Press, London, (1994).
7. R. Tycko, 'Biomolecular Solid State NMR: Advances in structural methodology and applications to Peptide and Protein Fibrils', *Annu. Rev. Phys. Chem.* 52, 1, pp. 575–606, (2001).

8. E. R. Andrew, A. Bradbury, R. G. Eades, 'Nuclear magnetic resonance spectra from a crystal rotated at high speed', *Nature* 182, 4650, pp. 1659–1659, (1958).
9. I. J. Lowe, 'Free induction decays of rotating solids', *Phys. Rev. Lett.* 2, 7, pp. 285–287, (1959).
10. S. R. Hartmann, E. L. Hahn, 'Nuclear double resonance in the rotating frame', *Phys. Rev.* 128, 5, pp. 2042–2053, (1962).
11. F. M. Lurie, C. P. Slichter, 'Spin temperature in nuclear double resonance', *Phys. Rev. A.* 133, 4, pp. 1108–1122, (1964).
12. A. Pines, M. G. Gibby, J. S. Waugh, 'Proton-enhanced NMR of dilute spins in solids', *J. Chem. Phys.* 59, 2, pp. 569–590, (1973).
13. E. Vinogradov, P. K. Madhu, S. Vega, 'Phase modulated Lee-Goldburg magic angle spinning proton nuclear magnetic resonance experiments in the solid state: A bimodal Floquet theoretical treatment', *J. Chem. Phys.* 115, 19, pp. 8983–9000, (2001).
14. M. Mehring, 'High Resolution NMR spectroscopy in solids', Springer-Verlag, Germany, (1976).
15. V. Royden, 'Measurement of the spin and gyromagnetic ratio of C^{13} by the collapse of spin-spin splitting', *Phys. Rev.* 96, 2, pp. 543–544, (1954).
16. A. L. Bloom, J. N. Shoorley, 'Effects of perturbing radiofrequency fields on nuclear spin coupling', *Phys. Rev.* 97, 5, pp. 1261–1265, (1955).
17. M. Mehring, A. Pines, W. K. Rhim, J. S. Waugh, 'Spin-decoupling in the resolution of chemical shifts in solids by pulsed NMR', *J. Chem. Phys.* 54, 7, pp. 3239–3240, (1971).
18. A. Samoson, E. Lippmaa, A. Pines, 'High resolution solid state NMR: Averaging of second-order effects by means of a double rotor', *Mol. Phys.* 65, 4, pp. 1013, (1988).
19. A. Llor, J. Virlet, 'Towards high-resolution NMR of more nuclei in solids: Sample spinning with time-dependent spinner axis angle', *Chem. Phys. Lett.* 152, 2, pp. 248–253, (1988).
20. B. F. Chmelka, K. T. Müller, A. Pines, J. Stebbins, Y. Wu, J. W. Zwanziger, 'Oxygen-17 NMR in solids by dynamic-angle spinning and double rotation', *Nature* 339, pp. 42–43, (1989).
21. L. Frydman, J. S. Harwood, 'Isotropic spectra of half-integer quadrupolar spins from bidimensional magic-angle spinning NMR', *J. Am. Chem. Soc.* 117, 19, pp. 5367–5368, (1995).
22. Z. Gan, 'Isotropic NMR spectra of half-integer quadrupolar nuclei using satellite transitions and magic-angle spinning', *J. Am. Chem. Soc.* 122, 13, pp. 3242–3243, (2000).
23. F. H. Larsen, N. C. Nielsen, 'Effects of finite RF pulses and sample spinning speed in multiple-quantum magic-angle spinning (MQ-MAS) and multiple-quantum quadrupolar Carr-Purcell-Meiboom-Gill magic-angle spinning (MQ-QCPMG-MAS) nuclear magnetic resonance of half-integer quadrupolar nuclei' *J. Phys. Chem. A.* 103, 50, pp. 10825–10832, (1997).
24. M. M. Maricq, J. S. Waugh, 'NMR in rotating solids', *J. Chem. Phys.* 70, 7, pp. 3300–3316, (1979).
25. B. C. Gerstein, C. Clor, R. G. Pembleton, R. C. Wilson, 'Utility of pulse nuclear magnetic resonance in studying protons in coals', *J. Phys. Chem.* 81, 6, pp. 565–570, (2001).
26. C. E. Bronnimann, B. L. Hawkings, M. Zhang, G. E. Maciel, 'Combined rotation and multiple pulse spectroscopy as an analytical proton nuclear magnetic resonance technique for solids', *Anal. Chem.* 60, 17, pp. 1743–1750, (1988).
27. M. L. Buszko, C. E. Bronnimann, G. E. Maciel, '^{1}H CRAMPS based on TREV', *J. Magn. Reson. A.* 103, 2, pp. 183–187, (1993).
28. M. Lee, W. I. Goldburg, 'Nuclear-magnetic-resonance line narrowing by a rotating RF field', *Phys. Rev. A.* 140, 4, pp. 1261–1271, (1965).
29. M. Howhy, N. C. Nielsen, 'Elimination of high order terms in multiple pulse nuclear magnetic resonance spectroscopy: Application to homonuclear decoupling in solids', *J. Chem. Phys.* 106, 18, pp. 7571–7586, (1997).
30. S. Paul, R. S. Thakur, P. K. Madhu, '^{1}H homonuclear dipolar decoupling at high magic-angle spinning frequencies with rotor-synchronised symmetry sequences', *Chem. Phys. Lett.* 456, 4–6, pp. 253–256, (2008).
31. J. P. Amoureux, B. Hu, J. Trébosc, 'Enhanced resolution in proton solid-state NMR with very-fast MAS experiments', *J. Magn. Reson.* 193, 2, pp. 305–307, (2008).
32. D. Sakellariou, A. Lesage, P. Hodgkinson, L. Emsley, 'Homonuclear dipolar decoupling in solid-state NMR using continuous phase modulation', *Chem. Phys. Lett.* 319, 3–4, pp. 253–260, (2000).
33. E. Vinogradov, P. K. Madhu, S. Vega, 'High-resolution proton solid-state NMR spectroscopy by phase-modulated Lee-Goldburg experiment', *Chem. Phys. Lett.* 314, 5–6, pp. 443–450, (1999).
34. M. Leskes, P. K. Madhu, S. Vega, 'A broad-banded z-rotation windowed phase-modulated Lee-Goldburg pulse sequence for ^{1}H spectroscopy in solid-state NMR', *Chem. Phys. Lett.* 447, 4–6, pp. 370–374, (2007).
35. S. Vega, 'Floquet theory', *The Encyclopedia of Nuclear Magnetic Resonance*, Wiley, London, pp. 2011–2025, (1995).
36. U. Haeberlen, 'High resolution NMR in solids — selective averaging', Supplement — 1, *Adv. Magn. Reson.*, Academic Press, New York, (1976).
37. J. S. Waugh, L. M. Huber, U. Haeberlen, 'Approach to high-resolution NMR in solids', *Phys. Rev. Lett.* 20, 5, pp. 180–182, (1968).
38. P. Mansfield, 'Symmetrized pulse sequences in high resolution NMR in solids', *J. Phys. C.* 4, 11, pp. 1444–1452, (1971).
39. D. P. Burum, M. Linder, R. R. Ernst, 'Low-power multipulse line narrowing in solid-state NMR', *J. Magn. Reson.* 44, 1, pp. 173–188, (1981).
40. K. Takegoshi, C. A. McDowell, 'A "magic echo" pulse sequence for the high-resolution NMR spectra of abundant spins in solids', *Chem. Phys. Lett.* 116, 2–3, pp. 100–104, (1985).
41. M. Howhy, P. V. Bower, H. J. Jakobsen, N. C. Nielsen, 'A high-order and broadband CRAMPS experiment using z-rotational decoupling', *Chem. Phys. Lett.* 273, 5–6, pp. 297–303, (1997).
42. M. Mehring, J. S. Waugh, 'Magic-angle NMR experiments in solids', *Phys. Rev. B.* 5, 9, pp. 3459–3471, (1972).
43. A. Bielecki, A. C. Kolbert, M. H. Levitt, 'Frequency-switched pulse sequences: Homonuclear decoupling and dilute spin NMR in solids', *Chem. Phys. Lett.* 155, 4–5, pp. 341–346, (1989).
44. M. H. Levitt, 'Symmetry-based pulse sequences in magic-angle spinning solid-state NMR', *Encyc. of NMR*, (D.M. Grant, R.K. Harris, Eds.), John Wiley & Sons, Chichester, (2002).
45. E. Salager, R. S. Stein, S. Steuernagel, A. Lesage, B. Eléna, L. Emsley, 'Enhanced sensitivity in high-resolution ^{1}H solid-state NMR spectroscopy with DUMBO dipolar decoupling under ultra-fast MAS', *Chem. Phys. Lett.* 469, 4–6, pp. 336–341, (2009).
46. M. Leskes, S. Steuernagel, D. Schneider, P. K. Madhu, S. Vega, 'Homonuclear dipolar decoupling at magic-angle spinning frequencies up to 65 kHz in solid-state nuclear magnetic resonance', *Chem. Phys. Lett.* 466, 1–3, pp. 95–99, (2008).
47. M. Leskes, P. K. Madhu, S. Vega, 'Why does PMLG proton decoupling work at 65 kHz MAS?', *J. Magn. Reson.* 199, 2, pp. 208–213, (2009).
48. J. P. Amoureux, B. Hu, J. Trébosc, Q. Wang, O. Lafon, F. Deng, 'Homonuclear dipolar decoupling schemes for fast MAS', *Solid-state NMR* 35, 1, pp. 19–24, (2009).
49. O. Lafon, Q. Wang, B. Hu, J. Trébosc, F. Deng, J. P. Amoureux, 'Proton-proton homonuclear dipolar decoupling in solid-state NMR using rotor-synchronized z-rotation pulse sequences', *J. Chem. Phys.* 130, 1, pp. 014504(1–13), (2009).
50. E. Vinogradov, P. K. Madhu, S. Vega, 'Strategies for high resolution proton spectroscopy in solid-state NMR', *Top. Curr. Chem.* 246, pp. 33–90, (2005).

51. D. G. Cory, 'A new multiple-pulse cycle for homonuclear dipolar decoupling', *J. Magn. Reson.* 94, 3, pp. 526–534, (1991).
52. A. Lesage, D. Sakellariou, S. Hediger, B. Eléna, P. Charmont, S. Steuernagel, L. Emsley, 'Experimental aspects of proton NMR spectroscopy in solids using phase-modulated homonuclear dipolar decoupling', *J. Magn. Reson.* 163, 1, pp. 105–113, (2003).
53. W. K. Rhim, A. Pines, J. S. Waugh, 'Time-reversal experiments in dipolar-coupled spin systems', *Phys. Rev. B.* 3, 3, pp. 684–696, (1971).
54. E. Vinogradov, P. K. Madhu, S. Vega, 'A bimodal Floquet analysis of phase modulated Lee-Goldburg high resolution proton magic angle spinning NMR experiments', *Chem. Phys. Lett.* 329, 3–4, pp. 207–214, (2000).
55. E. Vinogradov, P. K. Madhu, S. Vega, 'Proton spectroscopy in solid state nuclear magnetic resonance with windowed phase modulated Lee-Goldburg decoupling sequences', *Chem. Phys. Lett.* 354, 3–4, pp. 193–202, (2002).
56. L. Bosman, P. K. Madhu, S. Vega, E. Vinogradov, 'Improvement of homonuclear dipolar decoupling sequences in solid-state nuclear magnetic resonance utilising radiofrequency imperfections', *J. Magn. Reson.* 169, 1, pp. 39–48, (2004).
57. C. Coelho, J. Rocha, P. K. Madhu, L. Mafra, 'Practical aspects of Lee-Goldburg based CRAMPS techniques for high-resolution ^{1}H NMR spectroscopy in solids: Implementation and applications', *J. Magn. Reson.* 194, 2, pp. 264–282, (2008).
58. P. K. Madhu, 'High-resolution solid-state NMR spectroscopy of protons with homonuclear dipolar decoupling schemes under magic-angle spinning', *Solid state NMR*, 35, 1, pp. 2–11, (2009).
59. G. J. Boender, S. Vega, H. J. M. De Groot, 'A physical interpretation of the Floquet description of magic angle spinning nuclear magnetic resonance spectroscopy', *Mol. Phys.* 95, 5, pp. 921–934, (1998).
60. J. H. Van Vleck, 'On σ-type doubling and electron spin in the spectra of diatomic molecules', *Phys. Rev.* 33, 4, pp. 467–506, (1929).
61. M. Leskes, P. K. Madhu, S. Vega, 'Proton line narrowing in solid-state nuclear magnetic resonance: New insights from windowed phase-modulated Lee-Goldburg sequence', *J. Chem. Phys.* 125, 12, pp. 124506(1–18), (2006).
62. M. Leskes, P. K. Madhu, S. Vega, 'Supercycled homonuclear dipolar decoupling in solid-state NMR: Toward cleaner ^{1}H spectrum and higher spinning rates', *J. Chem. Phys.* 128, 5, pp. 052309(1–11), (2008).
63. P. K. Madhu, X. Zhao, M. H. Levitt, 'High-resolution ^{1}H NMR in the solid state using symmetry-based pulse sequences', *Chem. Phys. Lett.* 346, 1–2, pp. 142–148, (2001).
64. M. Veshtort, R. G. Griffin, 'SPINEVOLUTION: A powerful tool for the simulation of solid and liquid state NMR experiments', *J. Magn. Reson.* 178, 2, pp. 248–282, (2006).
65. M. Bak, J.T. Rasmussen, N.C. Nielsen, 'SIMPSON: A general simulation program for solid-state NMR spectroscopy', *J. Magn. Reson.* 147, 2, pp. 296–330, (2000).
66. B. Eléna, G. de Paepe, L. Emsley, 'Direct spectral optimisation of proton-proton homonuclear dipolar decoupling in solid-state NMR', *Chem. Phys. Lett.* 398, 4–6, pp. 532–538, (2004).
67. S. Paul, R. S. Thakur, M. Goswami, A. C. Sauerwein, S. Mamone, M. Concistré, H. Förster, M. H. Levitt, P.K. Madhu, 'Supercycled homonuclear dipolar decoupling sequences in solid-state NMR', *J. Magn. Reson.* 197, 1, pp. 14–19, (2009)
68. S. K. Zaremba, 'Good lattice points, discrepancy, and numerical integration', *Ann. Mat. Pura. Appl.* 73, pp. 293–317, (1976).
69. H. Conroy, 'Molecular Schrödinger equation. VIII. A new method for the evaluation of multidimensional integrals', *J. Chem. Phys.* 47, 12, pp. 5307–5318, (1967).
70. V. B. Cheng, H. H. Suzukawa Jr., M. Wolfsberg, 'Investigations of a nonrandom numerical method for multidimensional integration', *J. Chem. Phys.* 59, pp. 3992–3999, 8, (1973).

Subhradip Paul received his Bachelors degree in Chemistry Honours from St. Xavier's college, Kolkata, India, under the Calcutta University in 2006. Since 2006 he has been pursuing Ph.D. in Tata Institute of Fundamental Research. He has worked in the improvement of three-dimensional pulse schemes in solution-state NMR and his current research interests are in the area of homonuclear and heteronuclear dipolar decoupling in solid-state nuclear magnetic resonance.

P. K. Madhu did his Ph.D. with Anilkumar in Indian Institute of Science, Bangalore. He then did post-doctoral research with Shimon Vega, Weizmann Institute of Science, Israel, Norbert Mueller, University of Linz, Austria, and Malcolm Levitt, University of Southampton, UK. He has been a faculty in Tata Institute of Fundamental Research since 2003. P. K. Madhu's research interests are in developing methods to improve the resolution and sensitivity of solid-state NMR experiments.